Simulation of modeling of multi-megawatt photolvoltaic plants with high voltage direct current grid integration

Antonio Colmenar-Santos[a*] {acolmenar@ieec.uned.es}
Enrique Rosales-Asensio[b] {erosalea@ull.edu.es}
Enrique-Luis Molina-Ibáñez[a] {emolina37@gmail.com}
Jorge-Juan Blanes-Peiró[c] {jjblap@unileon.es}

[a] *Departamento de Ingeniería Eléctrica, Electrónica, Control, Telemática y Química Aplicada, Universidad Nacional de Educación a Distancia (UNED), Madrid, Spain*
Juan del Rosal, 12 – Ciudad Universitaria - Phone +34-913-987-788 ***Fax*** *+34-913-986-028*
[b] *Departamento de Física, Universidad de La Laguna, San Cristóbal de La Laguna, Spain*
[c] *Departamento de Ingeniería Eléctrica y de Sistemas y Automática, Escuela Técnica Superior de Ingenieros de Minas de LEÓN, Spain*

Abstract- *This paper develops an integrated model of multi megawatt PV plant with HVDC (High Voltage Direct Current) or HVAC (High Voltage Alternating Current) network, using the specific software of power electronics PSIM. This model has been developed by functional blocks, including the photovoltaic field itself, the pertinent conversion units for the integration of each network as well as the network type for production. The models allow to obtain transmissions loss for any combination of the three variables on which they depend; network length (km), temperature (ºC) and irradiance (W/m^2). To verify the validity of the model and demonstrate the distribution advantages of HVDC -even for relatively low-photovoltaic power plants in comparison to the common applications currently used in HVDC networks-, a case study has been used which has led to the conclusion that the use of HVDC networks may be convenient for this type of power generation plants.*

Keywords- *HVDC networks, photovoltaic integrated model, PSIM software, electric power transmission lines, power converter.*

ACRONYMS LIST

MMWPV	*Multi-megawatt Photovoltaic*
HVAC	*High Voltage Alternating Current*
HVDC	*High Voltage Direct Current*
HVDCGR	*High Voltage Direct Current Ground Return*
HVDCMR	*High Voltage Direct Current Metallic Return*
NOTC	*Nominal Operating Cell Temperature*
STC	*Standard Test Conditions*

I. INTRODUCTION

This research re-sparks the well-known *War of Currents* of the 19th century that had Edison, a proponent of DC and Tesla as the standard bearer of the AC [1]. From the current perspective, it is a challenge to discern a single winner; it is a long-established fact that such technological disagreement will result in a technical tie between both forms of electric transport and distribution, given the current technological momentum experienced by HVDC (*High Voltage Direct Current*) technology.

Such momentum arises from its advantages, highly contrasted and derived from the absence of the capacitive and inductive phenomena in AC networks. Such capabilities can be summarized as follows [2]:

- Great transport efficiency. DC can carry large amounts of electrical power over long distances.
- Flexibility as it permits asynchronous interconnections.
- Suitable for submarine links.

These great benefits have propelled the proliferation of HVDC networks and consequently gaining ground to alternating current by transporting and distributing more megawatts year after year. Proof of this is the number of complete HVDC projects, in progress or about to be completed. A few of these projects are emblematic. Two of these examples include the HVDC link DC voltage to ± 500 kV of 2004 in *Three Gorges (Guangdong, China)*, capable of transmitting 3000 MW over 940 km [3] or, the HVDC interconnection link between France and Spain of October 2015, which transmits ± 320 kV and 1400 MW of transport capacity [4].

Much like its advantages, there is a plethora of literature devoted to its disadvantages, the following are worth noting [2]:

- Higher cost of DC converters.
- Higher harmonic generation
- The intricate control employed in multi-terminal operations. The majority of the links are point-to-point.

But perhaps the main technical hurdle that has had to overcome HVDC technology has been the lack of a suitable switch [3]; when an AC switch is opened, an arc continues driving the current between the contacts to the next zero crossing. Since the DC current does not have this useful pass through the zero value of the current, a different approach is needed, and this has for a long time prevented the development of more complex HVDC network topologies [3].

However, these drawbacks are being addressed and or minimized by new switches capable of opening circuits with high alternating current, such as the hybrid switch developed by ABB. This switch combines semiconductor technology for the rapid interruption of DC with a fast mechanical switch [5]. In addition, the costs of the converter stations are decreasing, thanks to the increase of production in the sale of units and their greater integration in the market.

A direct consequence of HVDC's growing demand is the high expectations set forth by the sector in renewable energy generation based on its high efficiency in transportation and long distance transmission capabilities while incurring minimum transmission loss, giving Renewable Energies a fresh and hopeful boost. This is the case, for example, of the *TuNur project* [6], consisting of a large solar thermal plant that is intended to be built in the Sahara of Tunisia to supply electricity to Europe through an submarine cable of more than 600 km connected to the grid European in the Italian part.

In this instance, it makes sense to use photovoltaic power plants in direct current since PV modules already produce direct current electricity from sunlight. Additional factors encourage a paradigm shift in the distribution of energy generated in these plants. These factors are as follows;

- The increased proliferation of DC powered equipment, such as the electric car, or LED lighting has prompted the review of low-voltage electrical distribution, and in some cases is being considered to generating power straight into DC, developing networks with a greater efficiency and cost reduction [7].
- The birth of a new type of solar PV power stations, of floating type, on areas of water reservoir, such as the one in *Nishihira Pond* of 1,7 MW or 1,2 MW *Higashihara's pond*, both in the city of *Kato, Japan*, in operation since March 2015 [8]. This revolutionary design has increased production thanks to its cooling effect, solving the lack of space while reducing the evaporation of water reserves [9].
- Although the development of these floating photovoltaic fields is focused on reservoirs or the cited ponds, it opens the door for its use in maritime zones, emulating offshore wind farms. In fact, there are already PV modules on the high seas, prototypes and testing techniques for future use [10].
- In both cases, submarine type links would be required, and under these conditions, AC transport is limited to short distance, given the high capacitance of isolated conductors, as already indicated.

Unlike the typical applications of HVDC networks such as large and long-distance energy transports, connections between asynchronous systems and submarine links, this research has a different focus. This paper explores its use in similar networks such as the large photovoltaic power plants in the range of several megawatts, but with inferior power typically handled by HVDC links.

Therefore, the fundamental objective of this study is the development of a simulation model for a grid connected multi-megawatt photovoltaic plant and its different technologies HVAC and HVDC. Such model can precisely detect energy losses incurred during distribution based on two of three variables that affect transmission, with the fixed network length; temperature, and irradiance.

In this way, it will be possible to have a very useful tool in obtaining the critical distance of the links, in other words, the distance from which is most profitable to distribute in DC instead of AC, and that as a general rule is approximately between 800 and 900 km for aerial networks and 60 and 70 km for underground [11].

Another key aspect is verifying the suitability of small-scale HVDC links to distribute the production of multi-megawatt photovoltaic plants and determine if these plants can benefit from said advantages, which would undoubtedly lead to a greater integration and presence of Solar photovoltaic energy worldwide.

In *Section II*, the various stages of work -that have been covered to achieve the objectives set out in the first section- are discussed along with a technical analysis of the conditions and functional requisites for the integration of the MMWPV plants into HVDC networks. This analysis culminates in a proposal of unit converter plant MMWPV - Network HVDC that will lay the foundation for the rest of the study. Subsequently, two working models of MMWPV plant are developed, including both HVDC and HVAC networks, figures 2 and 3.

In *section III*, the models generated are applied to a specific case of MWPV plant, using real technical data of the integrating components and gathered from commercial catalogs. These elements have been previously modeled in a generic way (as already indicated) to obtain through the subsequent simulation the losses resulting from energy transportation according to the variables which define them including temperature (ºC) and irradiance (W/m^2), and considering a specific length. This section concludes with a summary of results, table IV.

Finally, *section IV* presents the most relevant conclusions based on the results including, the validity of the models, the technical and economic viability of the integration of MWPV into HVDC and the possible applications in both developed and developing countries.

II. MATERIALS AND METHODS

The simulation models were built upon a well differentiated four phase process:

1) The phase of research and analysis of the PV plant elements including - distribution networks, with emphasis on the current situation and future trends or lines of development, taking as references, besides those indicated, the technical documentation of the leading manufacturers in the transport sector in HVDC, *ABB*, and *Siemens*.
2) Block structured functional design of the required central converting unit (multi-megawatt photovoltaic plant connected to HVDC grid).
3) Modeling the system, using PSIM power electronics software, following a modular strategy; photovoltaic field, central converter unit MMW PV connected to HVDC grid, central converter unit MMW PV- HVAC, HVDC and HVAC distribution networks.
4) A case study to apply the generated models and subsequent simulations to measure transmit losses for any combination of the variables that affect transmission rate including, temperature (ºC) and irradiance (W/m^2), with a certain network length.
   These simulations will be tested on three types of networks (HVDC GR, Ground Return, HVDC MR, Metallic Return, and Three-phase HVAC), with aerial or underground lines.
   By following this process, all the possible cases will be covered, establishing the validity of the generated models, in addition while comparing transmit loss among these to showcase the advantages of HVDC transmission for PV plants, which fall under the category of small-scale plants for electric generation.

II.A.- FUNCTIONAL DESIGN CENTRAL CONVERTING UNIT MMWPV-HVDC NETWORK

To carry out the coupling of PV plants in HVDC networks it will be necessary a DC / HVDC converter capable of coupling the variable production in voltage and DC type and low voltage that occurs in the PV field to the high voltage requirements in continuous and variable current of the HVDC networks.

There are several alternatives to raise the voltage of the DC field, DC type and variable according to the environmental conditions, to the orders of magnitude of the order of kV required in the HVDC links (since the Joule effect losses decrease with the square of the tension). The alternatives are:

- Connect the strings of modules in series or strings. A no-viable option due to the limit of the inverse voltage in the PV modules, around the 1000 V.
- Connect the strings of modules in series or strings after the maximum power point tracker, MPPT or Maximum Power Point Tracker, which is also not viable because in practice it would disable its functionality, subduing all the modules to the maximum power generated by the chain of worst production.
- Another option could be including a boost converter (or booster) after the MPPT block; a structure already offered by a few current PV inverters without a transformer. These converters are

primarily used in regulated DC power sources and regenerative DC motor braking. As its name implies, the output voltage is always larger than the input voltage, and it includes a large output filter capacitor to ensure a constant output voltage [12]. This option, however, has two limitations; one in the amplification range, too short for the needed requirements and the other is low performance compared to DC / AC converters.

- From the standpoint of achieving equal performance to that of the DC / AC converters of the PV plants in AC networks, the best option to achieve the high output voltages of the PV-HVDC unit is, paradoxically, using an AC transformer. The proposed structure is similar to those seen in the current medium voltage photovoltaic plans or MMSS (Multi Megawatt Solar Station), but with an additional rectifier stage.

These platforms are making headway in the last two years favored by the programming and installation of the major photovoltaic systems, mainly in the United States, China and several countries in South America, in the order of several tens of megawatts [13].

Medium-voltage PV platforms power ranges from 300 kW to 2500 kW contain all the necessary elements to simplify the construction of high-power photovoltaic solar energy installations. These vary depending on the manufacturer parameters such as the number of MPPT trackers, the number and type of DC / AC converters, and the characteristics of the low to medium voltage transformer.

By adding a rectifier stage to one of these platforms, the outcome is a structure capable of satisfying the functional requirements, i.e., a high and constant DC tension, which will vary depending on the solar production of each moment. In other words, it is reversed to raise the tension and rectified to reap the benefits of transmission in HVDC.

This structure is a combination of two standalone systems; the medium voltage PV platform on one side and a small-scale AC / HVDC converter station of the order of megawatt with order output voltages of some tens of kV.

Therefore, this PV-HVDC unit must have (see Fig. 1):

- MPPT (maximum power point tracking) blocks, which are truly DC converters. These trackers are fundamental to increase the efficiency in the utilization of the production of the photovoltaic field. Much has been done in the recent years regarding improvements in control algorithms to improve tracking. One of the future trends may include tracking algorithms based on adaptive control techniques [14].
- Central type DC/AC converter units, given the many modules connected into the MMW PV plant; it is customary to have an inverter for every 500 kW approximately. It is proposed to use the three-phase VSI (voltage source inverter) type with SPWM (pulse width sinusoidal modulation), state-of-the-art control technology based on the utilization of multiple modulations with pulse width variation proportional to the amplitude of a sine wave evaluated at the center of said pulse [15]. Given the power requirements, this VSI inverter must use IGBT (Insulated Gate Bipolar) switches. There will be a constant value sine wave voltage at the output of these inverters along with a variable current which follows the current variations of the PV field.
- A single low to medium voltage transformer to collect the outputs of all the DC/AC converters the platform supports. A single transformer could be included for each inverter, but that would increase the final price. It is important to point out that a few types of medium-power grid-connected inverters include high-frequency transformers to boost performance to which the previous CC/CA bridge works at elevated frequencies.
- A final rectifier stage based on IGBT type devices is recommended, given the need to reach medium voltage tensions, this final stage must be composed of a multi-level converter of three levels, according to the Diode-Clamped topology also known as Neutral-Point-Clamped, with two

capacitors on the DC bus. Multilevel inverters are a breakthrough concerning traditional inverters, as these can handle large voltages and powers, generating alternating voltages with fewer harmonics than conventional inverters [16]. The diodes connected to the midpoint are the elements that set the blocking voltages of the switches at a fraction of the DC bus voltage, making these an essential component of this topology. During normal operations, there are two semiconductor switches per phase in a locked state, which allows double-voltage operation of the DC link of a two-level converter using the same elements. As a result, this converter/rectifier will allow working with output voltages in the medium voltage range, making the VSI bridge with IGBT combination the best choice [17].

Once the necessary conversion unit structure is selected, the next step is developing a valid functional model of all the elements that comprise the MMW PV plant, from the PV modules to the distribution network, to procure its integration into a single structure, which is also the final objective of this study.

The specialized power electronics software PSIM V11.0.3 [18] will be used for this purpose and a modeling line will be followed according to specific functional criteria specific to the elements that make up the installation (for example, the PV modules) together with the rules and electrotechnical laws that govern the electrical behavior of the assembly.

II.B.- MODELING OF THE PV FIELD AND THE MPPT BLOCK

As previously indicated, PSIM is a critical resource for this research and consequently for this modeling as it aids in the implementation of the photovoltaic field. This physical solar model can be found in PSIM's component library "Renewable Energy Module". This module factors the variation of solar radiation and temperature, which are fundamental to the analysis of losses during distribution under different environmental conditions (reference PV field in Fig. 2 & Fig. 3). PSIM PV model block was used to model our PV system and modelled the MPPT with an efficiency gain. The equivalent circuit that employs the physical model includes the equivalent circuit of a solar cell, along with the equations that characterize it [18].

Nevertheless, it is necessary to supply a large number of parameters. A few of these can be found in the manufacturer's data sheets as shown below;

- N_S, number of serially arranged cells which compose the module.
- V_{OC} (V), open circuit voltage.
- V_{MP} (V), the voltage at maximum power.
- I_{SC} (A), short-circuit current.
- I_{MP} (A), current at maximum power.
- P_{PMP} (W), maximum power, peak power or at the point of maximum power.
- V_{OC} temperature coefficient (%/ºC o K).
- I_{SC} temperature coefficient (%/ºC o K).
- (dv / di) in V_{OC} refers to the slope (dv / di) in the open circuit voltage V_{OC}, which can be estimated from the V-I characteristic curve of the solar module.

Table I displays other parameters, these parameters are not usually provided by the datasheet, so in [19] is presented how to obtain these parameters with the help of the I-V curve provided by the datasheet [20]. *Solar Module (Physical Model)* is another useful feature included in PSIM as it facilitates the definition of the solar module parameters described in section III.B, and display precisely the operation of the chosen module for the application case.

The MPPT block can be implemented following different control strategies, such as [21]:

- Method of disturbance and observation (D&O).
- Incremental conductance method.
- Hill Climbing Technique.
- MPPT method with current measurement.

The physical model of the PV panel that has been used to model the PV field, has 2 inputs, where the temperature and irradiance conditions of the module are set, and three outputs:

- One positive and one negative terminal to deliver the power the module is giving, per temperature and irradiance as well as the connected load.
- The third output is at the top, where maximum power point information is provided about those ambient conditions regardless of the connected load. This output will, therefore, be utilized since it is equipped with the maximum power point tracker.

A proportional block with a gain of 0,99 has been included to take into account the current performance of the MPPT devices, which is around 99%.

II.C.- PV-HVDC UNIT MODELING

At a functional level, the converter-transformer-rectifier unit behaves as a constant-current transducer, causing the HVDC output network to have a high voltage, of the order of kV, and a fixed value, and a current variable that follows the variations produced in the PV field. Therefore, a model has been developed based on the following criteria as indicated in figure 2:

- The use of an adder is required to sum the power produced by each of the converter units, providing us with the PPVT, total PV power. The value of the converter unit's performance can be included in each of the input gain, which can be estimated generically at 0,95.
- By adding a voltage-to-voltage transducer, it is possible to adapt the working voltage for the rest of the elements of the circuit. The gain of this transducer will be adjusted according to the working voltage of the HVDC network. Therefore, the amount of gain from the first transducer is a DC voltage of equal value to the PV current.

$$I_{MPPPV\ TOTAL} = \frac{PPVT}{V_{HDVC}} \quad (1)$$

- The next step involves another voltage-current transduction, adjusting the gain of this second transducer to the estimated transformer performance.

As a result, the PV-HDVC unit will have all the current produced by the PV field with the corresponding performances and the desired working voltage.

II. D.- PV-HVAC UNIT MODELING

The operation of MMW PV platforms with medium distribution AC system modeling is required to comparing transmit losses between the HVDC or HVAC networks. Such modeling calls for an alternating voltage generation with an effective value which corresponds to the working HVAC voltage and resistance that changes according to the PV output as indicated in figure 3.

The variation of the voltage's internal resistance based on production is equivalent to injecting more or less current into the HVAC network. The use of the *nonlinear element V = f (i, x)* is necessary to

consider the association of PV HVAC system to establish the parameters. In this equation, the PV power generation is the external variable based on environmental conditions.

$$V_{LINE\ HVAC} = f(i,x) = i_{phase} \cdot r_{i\ phase} = i_{PHASE} \cdot \frac{V_{HVDC}^2}{\left(\frac{PPVT}{\sqrt{3}}\right)} = \frac{i_{PHASE} \cdot V_{HVDC}^2 \cdot \sqrt{3}}{PPVT} \quad (2)$$

For the parameterization of the system it is necessary to know the voltage trend with respect to the intensity, as shown below;

$$\frac{\partial V_{LINE\ HVAC}}{\partial i} = \frac{V_{HVDC}^2 \cdot \sqrt{3}}{PPVT} \quad (3)$$

II. E.- HVDC NETWORK MODELING

Before modeling a monopolar link, there is a need to include a resistance that characterizes the ohmic value of the line, which will depend on the type of conductor, the distance between the link and the calculating section. The network model HVDCGR, nonlinear element v = f (i, x) is necessary to include the effect of the variation of the link length to establish the parameters. In this equation, the length is the external variable, which will change during the simulation from zero to the link's maximum distance.

$$V_{LINE\ HVDCGR} = f(i,l) = I \cdot R_{LINEHVDC} = i \cdot \rho \cdot \frac{l}{S}.1000 \quad (4)$$

The multiplication factor of 1000 is included to work in km. For the parameterization of the system it is necessary to know the voltage trend with respect to the intensity, as shown below;

$$\frac{\partial V_{LINE\ HVDCGR}}{\partial i} = \rho \cdot \frac{l}{S}.1000 \quad (5)$$

When modeling a monopolar link with a metallic return, it is only required to include the multiplication factor of 2 in expressions 4, and 5 since the distance to consider is doubled due to the use of two conductors in the link.

II.F.- HVAC NETWORK MODELING

The total inductive reactance value of each phase is estimated based on the data provided by the manufacturer for insulated cables, and design of aerial networks with bare conductors. Once this value is known and to determine the value of the required inductance all that is required is to apply the concept of reactance impedance:

$$X_{LPhase} = 2 \cdot \pi \cdot f \cdot L(H) \rightarrow L(H) = \frac{X_{LPhase}}{2 \cdot \pi \cdot 50} \quad (6)$$

II.G.- SIMULATION AND VARIABLE MODELING

Once the previously mentioned systems are modeled the full integration yields the following models: MMW PV-HDVC as seen in figure 2, and MMW PV-HVAC as seen in figure 3. Tables II and III specify the meaning of all external variables and measurement points for both models.

III. RESULTS AND DISCUSSION

III.A.- INSTALLATION DATA TO BE MODELED

Through modelling it might be able to estimate transmission losses for any combination of the variables that affect transmission including, temperature (ºC) and irradiance (W/m^2), with a certain network length. If no measurements were available, the best way to test the veracity of these models is by running simulations on a few actual case studies involving, a 2 MW PV power plant for HVDC and HVAC connection, a Ground Return HVDCGR and metallic return HVDCMR.

The baseline data includes:

- Types of distribution networks to be analyzed:
  - An 80-km underground distribution network built with insulated aluminum cables. Total transit loss will be calculated in the three modeled networks and different scenarios of irradiance and temperature.
  - An 80-km aerial distribution network built with bare aluminum cables. Total transit loss will be calculated in the three modeled networks and different scenarios of irradiance and temperature
- The following commercial elements will be considered for the parameterization of the model:
  - *ABB* medium-voltage PV array of 2MW nominal power, model PVS800-IS-2000kW-C with the following specifications for the parameterization purposes, are;
    - Number of MPPT units = 2
    - Number and type of inverter units: 2. Central inverter type. 2 x 1200 kW of maximum input power.
    - Number of inputs per inverter: 12
    - MPPT input voltage range: 600 to 850 V
    - Maximum input voltage: 1100V
  - Commercial PV module model NU-RC290 | 290 W from the manufacturer Sharp [20].
  - Medium-Voltage range commercial conductors, i.e., high-modulated ethylene-propylene insulated cables, called EPROTENAX will be used for the underground network. The technical specifications are extracted from [23]
  - Bare aluminum conductors, i.e., LA-XX type, will be used for the aerial network. The technical specifications are extracted from [23]
- Several case studies will be analyzed for each type of network (aerial or underground), and type of distribution technology (HVDCGR, HVDCMR, and HVAC), to establish a sound comparison of transmission losses between them. The cases consist of 4 relevant situations in each type of network according to the following alpha-numerical sequence: A (Aerial Network), U (Underground Network), Temperature (ºC) / Irradiance (W/m^2).
  - U/A Cases -10ºC/1000 (W/m^2), relevant cases because they representing the extreme limit of operation for the calculation of the upper limit of string couplings to the inverter units.
  - U/A Cases 25/1000 (W/m^2), relevant cases because they representing the standard conditions of measurement or STC.
  - U/A Cases 48/800 (W/m^2), relevant cases because they representing the normal operating temperature conditions of the cell, or NOTC.

- U/A Cases 70/1000 (W/m^2), relevant cases because they representing the extreme limit of operation for the calculation of the lower limit of string couplings to the inverter units.

These cases have been selected because they are very characteristic values in the PV studies in terms of irradiance and temperature, such as the STC and NOTC conditions. The other values are within the operating temperature of the electrical elements and meet the requirements of III.C. The value of -10ºC is due to the fact that in the Shetland Islands, the minimum registered temperature is -8.9ºC according to [24].

These simulations are carried out considering the distance variable of 80 km because it can be considered as an acceptable distance for PV installations on islands, floating or even in developing countries.

Once the general installation data is established, said data would then be parametrized in the generated models to calculate the transmission losses through simulation.

III.B.- SOLAR MODULE PARAMETRIZATION

The solar module used for this case is the module NU-RC290, manufactured by SHARP, consisting of 60 monocrystalline silicon cells connected in series [20].

It is necessary to use the tool *Solar Module (Physical Model)*, to transfer the functional characteristics of the module to the physical panel model. This process consists of the following steps [19].

III.B.1 DATASHEET INTRODUCTION

The basic electrical parameters I_{MPP}, V_{MPP}, I_{SC}, V_{OC}, P_{PMP}, the number of cells and temperature coefficients of I_{SC}, V_{OC}, are introduced.

The value "dv/di (slope) in V_{OC}" refers to the slope dv/di to the open-circuit voltage Voc, which can be approximated by the V-I curve of the module, obtaining an estimated value of -0,5.

III.B.2 INITIAL ESTIMATION OF EG, A, RSH, Y KS

Typically, these four parameters are not provided in the data sheet and have to be approximated.

According to the considerations of [19], in the case of the NU-RC290 module, we will assume initial values of: Eg = 1,12V, A = 2, Rsh = 2000 Ω, Ks = 0.

III.B.3 CALCULATING I-V P-V CURVES AND THE MAXIMUM POWER POINT

With the previous information, the tool calculates the following parameters: *series resistance* R_S, short-circuit current *Isc0*, saturation current *Is0*, and temperature coefficient *Ct*.

III.B.4 COMPARISON OF THE DATA SHEET AND EXPERIMENTAL DATA FOR DIFFERENT OPERATING CONDITIONS, AND PARAMETER ADJUSTMENT

Since the first parameter approximation is outside its nominal value in the catalog, it is necessary to fine tune the parameters A and (dv /di), generating a more accurate value which represents the selected module for the case study as shown in figure 4.

A fine-tuned parametrization reveals a closer value to that of the nominal power, which is 290,32W≈290W. These values are then loaded into the two physical panel models in the diagram, depicting the operation of the NU-RC290 module accurately.

III.C.- PHOTOVOLTAIC FIELD CONFIGURATION

Given the voltage at the output of the PV panels is a function of temperature, it is necessary to verify the inverter can operate in adverse conditions (-10 °C to +70 °C). The optimum coupling between the PV field and the inverter will, therefore, be guaranteed provided the followings conditions are met:

$$U_{\min PV}\left(@1000W/m^2\ y\ T^a = 70^oC\right) \geq U_{MPPT\min} \quad (7)$$

$$U_{\max PV}\left(@1000W/m^2\ y\ T^a = -10^oC\right) \leq U_{MPPT\max} \quad (8)$$

According to the module and inverter unit technical data sheets, the following apply:

- Solar module
  - UOC module= 39,3 V
  - Variation of Voltage with temperature: -0,29% / ºC.
- Inverter Unit MPPT data coupling
  - Inverter UMPPT min = 600 V
  - Inverter UMPPT max = 850 V
  - Inverter U max = 1100V

The previously mentioned conditions-presented in 7 and 8- can be verified by serially connecting the modules; however, in this instance and since each inverter unit is equipped with 12 inputs, it is necessary to interconnect these in 17 parallel strings, consisting of 20 modules per string.

$$20\ \left(\frac{modules}{string}\right) \times 17\ \left(\frac{string}{paralell}\right) \times 12\ \left(\frac{inputs}{inverter}\right) = 4080\left(\frac{modules}{inverter}\right) \quad (9)$$

Thus, the maximum total power for each inverter unit will be as follows:

$$P_{TOTAL\ INVERTER} = 4080\left(\frac{modules}{inverter}\right) \times 290\ \left(\frac{Wp}{module}\right) = 1\,183\,200\,W \approx 1200kW \quad (10)$$

Before implementing this PV field distribution in the model, the following must occur:

- The 20-module series per strings is configured by multiplying the number of cells of each physical model by 20:

$$20\ \left(\frac{modules}{string}\right) \times 60\ \left(\frac{cells}{module}\right) = 1200\left(\frac{cells}{string}\right) \quad (11)$$

- The parallel association of the 17 module strings series and the connection to each of the 12 inputs is configured by including the proportional block called Nstring (see figures 2 and 3) with equal gain is shown below:

$$N_{STRINGS} = 4080(\text{modules/inverter})/20\ (\text{modules/string}) = 204\,(strings/inverter) \quad (12)$$

III.D.- FV-HVDC CONVERTER UNIT SETTINGS

Once both PV module parameterization and PV array configuration are complete, the next step involves the parameterization of the FV-HVDC converter. Given the simplicity of the implemented model, only the desired HVDC voltage must be included. Such voltage is included in the transducer gain block power PV to tension (see figures 2 and 3).

There must be a correlation between the power and the voltage carried. Ideally, it is best to work at the highest allowed voltages, as losses due to the Joule effect decrease with the square of it. Furthermore, it is equally important to consider the range of standard distribution voltages.

A good way to approximate the appropriate voltage value in a distribution is by using the *Still* expression

$$U_{NETWORK}(kV) = 5{,}5 \cdot \sqrt{\frac{0{,}62 \cdot l + P}{100}} = 24{,}8kV \tag{13}$$

Therefore,

U voltage between phases, in kV

l line length in km

P Average power to be transmitted in kW

The distribution voltage of 20 kV, 20 000 V is a very common distribution voltage. It also matches that of the power to be transmitted. Therefore, the transductor gain power-voltage model should be configured as follows;

$$G_{TRANSDUCTOR\ PPV\ to\ V} = V_{RED\ HVDC} = V_{RMS\ RED\ HVAC} = 20kV \tag{14}$$

III.E.- PV-HVAC CONVERTER UNIT SETTINGS

The PV-HVAC converter unit settings involve the parametrization of the generator's internal resistance of 20 000V between lines to correlate as already indicated, the PV production into an HVAC network. By applying the expression (2), the nonlinear riphase resistance must be parametrized. The external variable is the generated PV power along with the already known working voltage of 20kV as shown below:

$$V_{LINE\ HVAC} = f(i,x) = i_{phase} \cdot r_{i\ phase} = i_{PHASE} \cdot \frac{V_{HVDC}^2}{\left(\frac{PPVT}{\sqrt{3}}\right)} = \frac{i_{PHASE} \cdot 20\,000^2 \cdot \sqrt{3}}{PPVT} \tag{15}$$

For the parameterization of the system it is necessary to know the voltage trend with respect to the intensity, which is:

$$\frac{\partial V_{LINE\ HVAC}}{\partial i} = \frac{20\,000^2 \cdot \sqrt{3}}{PPVT} \tag{16}$$

III.F.- UNDERGROUND NETWORK PARAMETERIZATION

The total length of the underground network is 80 km, and it consists of 20 kV insulated cables suitable for underground or underwater applications.

The following data is required to model the pertinent circuit for the underground network:

- Calculating conductor sections to obtain the resistance for HVDCGR and HVDCMR respectively.
- Inductive reactance X_L and capacity C equivalent per km and per phase are both necessary to model the three-phase HVAC link along with the resistance value obtained in the previous case.

The calculation of the section requires-given the length of the link and economic criteria to reducing values to acceptable values- the use of higher sections of those technically required based on the criteria of nominal load currents and short circuit current. It is important to remember that the voltage drop criterion has no bearing when calculating the section in a medium voltage network.

- As a starting point, power losses (associated with the heating of the conductors) is around 3% in the HVDCGR case.
- The previously calculated section will be used to compare the losses in the three types of links.

Considering the fundamental equation of transport as shown below [25]:

$$Losses(\%) = K \cdot \frac{l}{S} \cdot \frac{P_1}{U_1^2} \tag{17}$$

Therefore,

- K = Coefficient which depends on the line type.
- l = Length of the line.
- S = Section of the conductor used.
- P1 = Power measured at the source.
- U1 = Voltage measured at the source.

The coefficient K has the following value:

- DC lines: $K = 2\rho$
- Single-phase AC lines:. $K = \frac{2\,\rho}{cos^2\varphi_1}$
- Three-phase AC lines: $K = \frac{\rho}{cos^2\varphi_1}$

Its application reveals that in order to limit losses in an aluminum line to 3%, with a resistivity of 1/28 (m / Ω mm^2) at 90 ºC; therefore, a section of 476 mm^2 is required:

$$S = \frac{1}{28} \cdot \frac{80\,000}{0{,}03} \cdot \frac{2\,000\,000}{20\,000^2} = 476\,mm^2 \tag{18}$$

In this case, a section greater than 500 mm^2 is appropriate to minimize losses at the end of the HVDC GR run (80 km). It is a suitable section based on the total transport length (abnormally high) for the (small-scale) range of power to be distributed, especially when the purpose is to compare both networks, HVDC and HVAC.

The cable specifications reveal the inductance and capacity of the lines. In this case, and according to the specifications obtained in [23], the following information applies;

- The chosen section can handle a much higher current than the one circulating for each case, as clearly indicated by the economic criterion to minimize transmission losses.
- The same applies to the intensity criterion of the short-circuit current.
- The capacity of the cable, according to the manufacturer's data is 0,484 (µF/km), reactance at 0,095 (Ω/km), and in the case of three unipolar cables, the value is of 500 mm^2. These values are acceptable values because of the high capacitance and a low reactance, typical characteristics of insulated wires.

The parameterization of the nonlinear Rline resistance is required in the HVDCGR case to adjust the length during the simulations. Considering a maximum operating temperature of 90 ºC and aluminum conductor and applying (4):

$$V_{LINE\ HVDCGR} = f(i,l) = I \cdot R_{LINEHVDC} = i \cdot \rho \cdot \frac{l}{S}.1000 = i \cdot \frac{1}{28} \cdot \frac{l}{500}.1000 \tag{19}$$

For the parameterization of the system it is necessary to know the voltage trend with respect to the intensity, which is:

$$\frac{\partial V_{LINE\ HVAC}}{\partial i} = \frac{1}{28} \cdot \frac{l}{500}.1000 \tag{20}$$

For the modeling of the underground HVAC network, the following will be considered:

- Nonlinear and variable resistance with the length of each phase is modeled just like the HVDCGR, parameterization equations (19) and (20) since it is the same section, same conductor and same distance.
- In the case of an underground line with a high capacitance factor per km, the switches S1 and S2 connecting the capacitors at the ends of the configuration to "pi" shall be closed, assigning each a value of:

$$C_{LINE/2} = \frac{0{,}484 \times 80}{2} = 19{,}36 \mu F \tag{21}$$

- The inductance value of the line shall be, applying (6), and considering a factor of 0,095 (Ω/km) and a length of 80 km:

$$X_{LPhase} = 2 \cdot \pi \cdot f \cdot L(H) \rightarrow L(H) = \frac{0{,}095 \times 80}{2 \cdot \pi \cdot 50} = 24{,}19 mH \tag{22}$$

III.G.- AERIAL NETWORK PARAMETERIZATION

The aerial network is 80 km and must use bare 20 kV cables between phases, in addition to the supports and other elements necessary for its layout. The design includes a simple symmetric phase in a triangle. A commercial example of suitable cables for medium voltage aerial distribution is bare aluminum cables type LA-XX. The technical specifications can be extracted from [23].

The commercial section closest to that calculated based on economic criteria is 500 mm2 for underground networks, so the same example will be used again to achieve a more homogeneous comparison. A bare aluminum conductor with a 500 mm^2 section.

From this aluminum section and considering the link's length, upgrading HVDC networks is like the one underground.

The following must be considered when modeling an HVAC aerial network:

- Nonlinear and variable resistance with the length of each phase is modeled as in the case of HVDC GR, parametrization equations (19) and (20) since it is the same section, same conductor and same distance.
- Since it is a short-length aerial line with bare conductors, the effect of the capacitance can be ignored. As a result, switches S1 and S2−connecting the capacitors at the ends based on the "pi" configuration−will open.
- The line's inductance value shall be, applying (6), considering a factor of 0,35 (Ω/km), a common value for aerial lines with a symmetrical in equilateral triangle design [13] and a length of 80 km:

$$X_{LPhase} = 2 \cdot \pi \cdot f \cdot L(H) \rightarrow L(H) = \frac{0{,}35 \times 80}{2 \cdot \pi \cdot 50} = 89{,}12 mH \tag{23}$$

III.H.- SIMULATION SETTINGS

Once the necessary operations are performed to parameterize all the elements of both models, there is a need to adjust the parameters and begin the simulation.

III.I.1 SETTINGS OF THE TEMPORARY PARAMETERS OF THE SIMULATION

The temporary parameters for the graphical simulation are adjusted through the *Simulation Control tool*. Samples will be taken every 0,001 seconds. The entire simulation involving all variables will last 20 seconds.

III.I.2 VOLTAGE (V) -IRRADIANCE (W/m^2) TRANSDUCTION

The solar modules reach a working voltage level starting at a small little irradiance value, typically from 2 to 8 (mW /cm^2). An intermediate starting point 50 (W/m^2) will be taken, and therefore the voltage line required to cover the irradiance range, from 50 to 1000 (W/m^2), must be set to 20 seconds of simulation, as:

$$u(t)_{\rightarrow I(W/m^2)} = 50 + \frac{1000-50}{20} \cdot t = 50 + 47{,}5 \cdot t \tag{24}$$

III.I.3 VOLTAGE (V)-LENGTH TRANSDUCTION (km)

Likewise, the voltage line required to cover the entire length range, from 0 to 80 km should be characterized- for 20 seconds of simulation- as follows

$$u(t)_{\rightarrow l(Km)} = \frac{80}{20} \cdot t = 20 \cdot t \tag{25}$$

III.I.- UNDERGROUND NETWORK SIMULATION

The simulation results of the 4 developed cases of underground distribution for the three analyzed networks are summarized in Table IV. To show the ability to adapt of the generated models, two graphs generated during the simulation process of the underground network conditions, figures 5 and 6, are also included. Figure 5 shows the power loss progression associated with the Joule effect, which occurs in each of the networks (HVDCGR, HVDRMR, and HVAC) for a temperature of 25ºC, a total length of 80 km according to irradiance every step of the way, from 50 to 1000 (W/m^2).

The power loss progression is of quadratic nature since the losses are proportional to the square of the network's current, and it increases linearly with the increase of irradiance.

Figure 6 shows the progression of diminished capacity in the HVAC network, for a temperature of 25 °C, a total length of 80 km and an irradiance of 1000 (W/m^2).

The graph shows a significant peak of power demanded at the beginning, which is necessary to charge the lines, diminishing its capacity due to the reactive energy required to charge/discharge both the capacitance of the lines and its inductance.

III.J.- AERIAL NETWORK SIMULATION

The simulation results of the 4 developed cases of aerial distribution for the three analyzed networks are in Table IV. This case includes two graphs generated during the simulation process of the aerial network (see figures 7 and 8).

Figure 7 shows the power loss progression, associated with the Joule effect, given in each of the networks (HVDCGR, HVDCMR, and HVAC) for a temperature of 48ºC, an irradiance of 800 (W/m^2) according to length variation from 0 to 80 km. The graph shows the progression of such losses, which is of quadratic nature since the losses are proportional to the lines' ohmic effect, and this one increases proportionally to the length.

Figure 8 shows the progression of diminished capacity in an HVAC aerial network and for a temperature of 48 ºC in the cell, a total length of 80 km and an irradiance of 800 (W/m^2). Once again, the graph shows a significant peak of power demanded at the beginning, which is necessary to charge the lines, diminishing its capacity due to the reactive energy required to charge/discharge both the capacitance of the lines and its inductance.

III.K.- SUMMARY RESULTS

Table IV shows the summary of the results obtained in each of the four cases through a series of simulations, including the underground and aerial distribution networks, considering the total length for all three network types. These scenarios were selected because these are particularly significant in the photovoltaic power generation field of study.

From the results obtained, and given that an equal conductor cross section was used for the three types of networks in both types of distribution (500 mm^2), the following evaluations can be made;

- The network with fewest losses is the HVDCGR network since the link uses one single conductor. The losses in the HVDCMR system are of double digits in all cases, which is logical taking since the link has two conductors.
- The link with the most losses due to Joule effect is the HVDCMR, which is logical taking into account that such link carries all the current along two conductors and the HVAC the current is distributed through each phase in a relation less than $\sqrt{3}$.
- Joule losses in HVDCGR and HVAC are very similar, with greater differences in the case of underground distribution. The following should be noted:
    - In a real situation and due to the skin effect, the resistance of the phases in AC will be somewhat higher; therefore, one may think the difference between them is due to this effect. However, and given that the models for such resistive effects −of both networks− have been characterized in the same manner, with a nonlinear resistance which value increases with length, the skin effect is ignored.
    - After this simplification, and given that in each phase a $\sqrt{3}$ smaller current is circulating and the total losses are the sum of the three phases and, in the absence of capacitive and inductive phenomena, the losses in both cases must be equal:

$$JL_{HVDCGR} = R_{LINE} \cdot I^2_{PV\,to\,NETWORK} \approx JL_{HVAC} = 3 \cdot R_{LINE} \cdot \left(\frac{I_{PV\,to\,Network}}{\sqrt{3}} \right)^2 \quad (26)$$

      If these are not equal, it is because of the capacitive and inductive effects of the lines. This difference is more noticeable in underground networks, with a high capacitance. The constant loading/unloading on the lines increases the current on the line, experiencing a greater transmission loss. In the aerial line case- having neglected this effect and given a shorter line- the effect is smaller, and the losses are similar.
- In addition to the Joule effect losses, HVAC networks experience transmission losses due to a reduction in capacity, moreover HVAC aerial networks have an inductive reactance, 10 times greater, which is supporting evidence that the losses due to the Joule effect- decrease capacity lead to higher transmission losses in HVAC to those in the HVDC network.
- Both types of losses involve a financial cost: Joule losses represent a direct economic cost and capacity reductions indirect costs of under-utilization, which is necessary to capitalize on as operating expenses.

The best and most efficient option in the transport of production of the 2 MW PV plant is the use of an HVDC GR networks as it experiences the lowest losses of all and it only requires one conductor, followed by HVDC with a metallic return, which have a lower transit loss (collectively) and uses one less conductor. These findings are not only insightful, but are also a fundamental to objective of this study− the development of a simulation model for multi-megawatt photovoltaic plant and its different technologies HVAC and HVDC− to precisely detect transmit losses according to temperature and irradiance, with a certain network length.

Along with the simulations carried out, a Joule loss analysis was carried out for the three network types underground with real data of the indicated location, the Shetland Islands, with irradiation data obtained from [26]. The selected data are those of the average irradiance of the month of July, with the objective of having significant data since the Shetland Islands are slightly above 60 ° N of latitude. The results are shown in figure 9. These findings culminate this research by drawing four very distinct, yet related conclusions. Findings have been compared with those available in top international journals [27-32] for comparative and validity purposes.

So far, little has been written in the scientific literature (in top international journals) about modeling multi-megawatt photolvoltaic plants. To our knowledge, state-of-the-art of previous modeling of multi-megawatt photolvoltaic plants has limited to using a wavelet variability model (WVM) for simulating solar photovoltaic (PV) power plant outputs (given a single irradiance point sensor timeseries using spatio-temporal correlations). See, for example, Lave et al. [33]; or to propose new control strategies that enable the storage requirements to smooth out short-term power fluctuations. See, for example, de la Parra et al. [34]. As a consequence, authors can reasonably prove that this paper incorporates some features that falls outside the pool of existing knowledge of its technical realm, which makes this paper of particular interest.

IV. CONCLUSIONS

The first conclusion relates to the generated models used in this research. Such models have adequately measured the transmission losses for any combination of the variables according to temperature, irradiance, and with a certain network length by evaluating and comparing the viable transport distances for HVAC, HVDC while allowing the length adjustment of said links. Moreover, these models have quantified performance variation in MMW PV plants at different temperatures; critical to accurately determining the increase in production as well as the losses incurred from changes in irradiation by applying irradiance variation's profile and adjusting the time during simulation, obtaining the total energy loss (Wh). Another key aspect of these models is the development of a tool that allows capitalizing the operating costs of the PV plant networks based on a multitude of combinations of said variables, simplifying the calculation of the various links' critical distance, thus making this process more efficient. Last, the modular nature of these models offers scalability for other PV plant configurations while making its parametrization simple as evident in the case study.

Next is technical feasibility of MMV PV plant integration in HDVC networks. The distribution of energy produced in MMW PV plants via HVDC networks is technically viable. These networks would work in the 15 to 30 kV range and power in the order of MW, which is considered a small-scale HVDC network.

Given the evidence presented in this paper, the best alternative for electrical distribution are HVDC networks a ground return as the first choice and metallic return as the second option, due to the decrese of capacity of the HVAC networks. Regarding the efficiency of the PV field converter unit, the most

efficient one is the combination of the existing medium voltage multi-megawatt PV with the addition of a final rectifier stage, as a small-scale HVDC converter station. This last state – given the power and voltage requirements– can consist of a multi-level structure IGBT type switches given the ranges of medium voltage output voltages required by the links. The last point involves transmission losses; therefore, and given both the thermal losses of the Joule effect and diminished capacity present in HVAC networks–resulting in line availability– it is concluded that, as a whole, the HVAC lines experience greater losses than the HVDCGR. Thus, the smaller scale environment PV plants operate under is more convenient to transport via the HVDC network.

The answer to the economic feasibility of the use of MMW PV plants in HVDC networks is that for HVDC transport to be economically viable, the cost between the two transport options must level. It will happen when the savings resulting from the reduction of conductors and transit losses equals that of the multilevel rectifier unit plus the cost of the end-of-line converter station, which is becoming increasingly feasible because of substantial cost reductions in power electronics and the small-scale power being handled.

The last differentiated yet related conclusion relates to MMW PV applications via HDVC networks. The output produced by -MMW PV integrated into small scale HVDC networks- offers a myriad of possibilities including market penetration. One of these involves the use of floating PV plants in reservoirs or islands close to the shore, using one single conductor, decreasing losses as already demonstrated. Another possibility has the potential to become a very viable alternative to increase the electrification rate of developing countries, given the reduction of costs that can be achieved, the large transport distances that can be reached for distributed systems and the great solar capital available in the majority of these.

ACKNOWLEDGMENTS

Thank to María Guindulain Argandoña for her collaboration in the translation of the article, which has been of great heppful and a great boost in the stage final of this paper.

APPENDICES

APPENDIX A. HVDC NETWORK MODELING

There are different interconnection topologies between the converter stations in HVDC networks. Given the complexity of the multi-terminal control, the most common use, as already indicated, it is the point-to-point interconnection. The number of cables interconnecting stations varies. The most common are;

- Monopolar links with *Ground Return*, *HVDCGR*. It uses a single conductor to transmit electrical energy. The return uses connected electrodes, which are in turn connected to the conversion stations. These electrodes perform the functions of anode and cathode. This type of connection connects systems separated by long distances and where the non-installation of the return cable can lead to considerable savings [2].

- Homopolar links with a metallic return, *HVDCMR*. A few monopolar systems include a metallic return when grounded electrodes are not an option, typically because of environmental issues, or when losses are significant [2].
- Bipolar links are currently used the most for its greater power transmission capacity.

Ground return monopole systems are simpler and cheaper than other systems and are best suited for moderate energy transfer [4]. Therefore, in the case of MWPV plants, the most suitable link is monopolar, given the small-scale level of the power to be transmitted.

APPENDIX B. HVAC NETWORK MODELING

When modeling AC lines of medium to long length or in all distances when it comes to AC underground lines, it is important to consider three factors. These include the effects exerted by both the resistance and the inductance, and most importantly, the effect of capacity; responsible for leakage currents, capable of decreasing transport capacity until it is rendered unfeasible. The T-equivalent circuit method or the "Pi" method can be used to consider these effects [22].

The "Pi" method is suitable as it provides greater versatility in simulations, see figure 34, with the half capacitances connected in parallel through two manual switches S1 and S2. These switches are connected according to the length of the line, that is, depending on whether or not the capacitive effects can be ignored.

For the characterization of these parameters, it is necessary to consider:

- The ohmic value determines the resistance for each phase, and it includes the variable length, just as in the case of the HVDCGR or HVDCMR. Because of the skin effect present in AC, there is more current flowing around the periphery of the conductor, so the total resistive value of the line is higher, but this effect has no relevance in low frequencies such as 500.95
- work of the link.
- Despite conductance's (G) ability to measure the leakage current of both the insulators and those due to the corona discharge, it is not used in many case studies because conductance's incidence is low under normal operations conditions and is complicated to calculate. As a result, it is often disregarded and considered to be infinite.
- The total inductive reactance value of each phase is estimated following II.F.
- The manufacturer’s data is needed to determine the value of the network capacity required for the model. The data includes isolated conductors, and it is calculated according to the design of aerial networks with bare conductors as previously mentioned.

REFERENCES

[1] Francescutti P. La guerra de las Corrientes. Available from: http://www.ree.es/sala_prensa/ext_img/entrelineas-0007_5.pdf [Accessed December 28th 2017].

[2] Bahrman M and Johnson B. The ABCs of HVDC transmission technologies. IEEE Power and Energy Magazine. 2007;52(2):32-44.

[3] Moglestue A. 60 years of HVDC. ABB Review. 2014; (2):33−41

[4] Red Eléctrica de España. Interconexión subterránea España-Francia. Available from http://www.ree.es/es/actividades/proyectos-singulares/nueva-interconexion-electrica-con-francia [Accessed December 28th 2017].

[5] Ohlsson D, Korbel, J, Steiger U. Opening move. ABB Review. 2013; (3):27−33

[6] Llamas D. Proyecto para llevar energía termosolar desde Sáhara Europa. Available from: http://helionoticias.es/proyecto-para-llevar-energia-termosolar-desde-el-sahara-hasta-europa/ [Accessed December 28th 2017].
[7] Ministerio de Economia y competitividad. Congreso Iberoamericano sobre Microrredes con Generación Distribuida de Renovables, October 11-13, 2012, Centro de Investigaciones Energeticas Medioambientales y technologicas, Soria, España; 2012
[8] Ruiz P. Se inauguran en Japón dos grandes centrales solares flotantes. Available from: https://www.energias-renovables.com/fotovoltaica/se-inauguran-en-japon-dos-grandes-centrales-20150519 [Accessed 28th July 2017].
[9] XVI Congreso Internacional de Ingenieria de Proyectos. Cubrición de embalses mediante un sistema de cubierta flotante fotovoltaico: análisis técnico y económico, July 11-13, 2014, Universidad Politecnica de Valencia, Valencia, España; 2014
[10] Serrano A. El nuevo reto de la Energía Solar. Available from: http://www.imf-formacion.com/blog/energias-renovables/articulos/energias-renovables-articluos/energia-solar/ [Accessed: December 28th 2017].
[11] Frau J, Gutiérrez J, Transporte de energía eléctrica en corriente continua: HVDC. Estado actual y perspectivas. Electrónica De Potencia, automática e instrumentación. 2005;(361): 2−14.
[12] Mohan N, Undeland T, Robbins W. Electrónica de potencia: convertidores, aplicaciones y diseño. 3th ed. Mexico. McGraw-Hill;2009.
[13] Salas Merino V, Olías Ruiz E, Grupo de Sistemas Electrónicos de Potencia, Departamento de Tecnología Electrónica, Universidad Carlos III de Madrid. Análisis de las grandes estaciones de potencia fotovoltaicas (multi megavatios) de media tensión.2013. Available from: http://www.jemaenergy.com/images/about/press/Instalaciones-en-grandes-plantas-fotovoltaicas-de-conexion-a-red.pdf [Accessed: December 29th 2017].
[14] Saavedra Montes A, Ramos C, and Trejos Grisales L. Adaptive maximum power point tracking algorithm for multi-variable applications in photovoltaic arrays. Journal EIA. 2013; 10 (20): 193-206. Available from: http://www.scielo.org.co/pdf/eia/n20/n20a17.pdf [Accessed: December 29th 2017].
[15] Gonzalez-Longatt F. Modulación Por Ancho de Pulso. 2004. Available from: http://fglongatt.org/OLD/Reportes/PRT2004-02.pdf [Accessed: December 29th 2017]
[16] Bueno E, Garcia R, Marrón M, and Urena J. et al. Modulation Techniques Comparison for Three Levels VSI Converters. In: 28th Annual Conference IEEE Industrial Electronics Society.Sevilla (Spain). IEEE. 20 March 2003. pp. 908-913. Available from: DOI 10.1109/IECON.2002.1185393
[17] Rashwan M. State of the VSC technology. [Presentation] IEEE 2011 Electrical Power and Energy Conference. October 2011.
[18] Powersim Software AS. PSIM User's Guide. Version 11.0. May 2017
[19] Powersim Software AS. Solar Module Physical Model Tutorial. Version 11.0. October 2016
[20] Datasheet NU-RC290 | 290 W, SHARP. Available from: https://eng.sfe-solar.com/wp-content/uploads/2016/03/SHARP_NURC290W_Mono_EN.pdf [Accessed: December 29th 2017].
[21] Fernandez H. Convertidores de potencia Aplicaciones y Análisis con el PSIM. Madrid: Kindle;2014.
[22] Mujal-Rosas R. Cálculo de líneas y redes eléctricas. Barcelona: Ediciones de la Universidad Politécnica de Catalunya;2002.
[23] PRYSMIAN SPAIN, S.A. Cables y Accesorios para Media Tensión. July 2014.
[24] Database of weather in the UK. http://www.weather.org.uk/climate/scotclim.html [Accessed: December 29th 2017].
[25] Fayos-Alvarez A. Líneas eléctricas y transporte de energía eléctrica. Valencia: Universidad Politécnica de Valencia;2013
[26] World Radiation Data Centre. http://wrdc.mgo.rssi.ru/wrdc_en_new.htm [Accessed: December 29th 2017]
[27] Kalair A, Abas N, Kalair AR, Saleem Z, Khan N. Review of harmonic analysis, modeling and mitigation techniques. Renewable and Sustainable Energy Reviews 2017;78:1152-1187.
[28] Aliyu AK, Modu B, Tan CW. A review of renewable energy development in Africa: A focus in South Africa, Egypt and Nigeria. Renewable and Sustainable Energy Reviews 2018;81(2):2502-2518.
[29] IqtiyaniIlham N, Hasanuzzaman M, Hosenuzzaman M. European smart grid prospects, policies, and challenges. Renewable and Sustainable Energy Reviews 2017;67:776-790.

[30] Dadhania A, Venkatesh B, Nassif AB, Sood VK. Modeling of doubly fed induction generators for distribution system power flow analysis. International Journal of Electrical Power & Energy Systems 2013;53:576-583.
[31] Brennand TP. Renewable energy in the United Kingdom: policies and prospects. Energy for Sustainable Development 2004;8(1):82-92.
[32] Lior N. Sustainable energy development: The present (2009) situation and possible paths to the future. Energy2010;35(10):3976-3994.
[33] Lave M, Kleissl J, Stein JS. A wavelet-based variability model (WVM) for solar PV power plants. IEEE Transactions on Sustainable Energy 2013;4(2):501-509.
[34] de la Parra I, Marcos J, García M, Marroyo L. Control strategies to use the minimum energy storage requirement for PV power ramp-rate control. Solar Energy 2015;111:332-343.

Figure

FIGURES

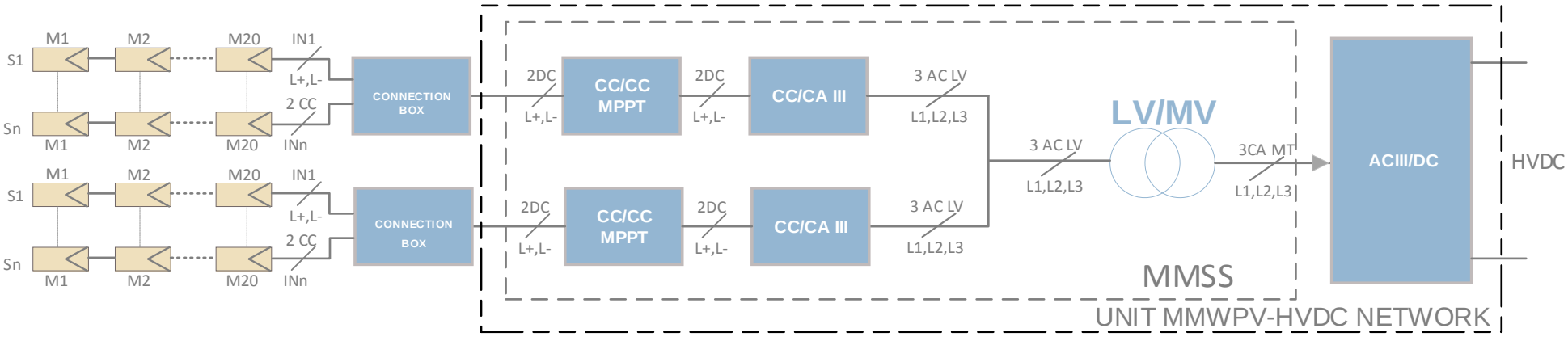

Fig. 1 Functional block diagram of the proposed MMWPV-HVDC station [Self-developed]

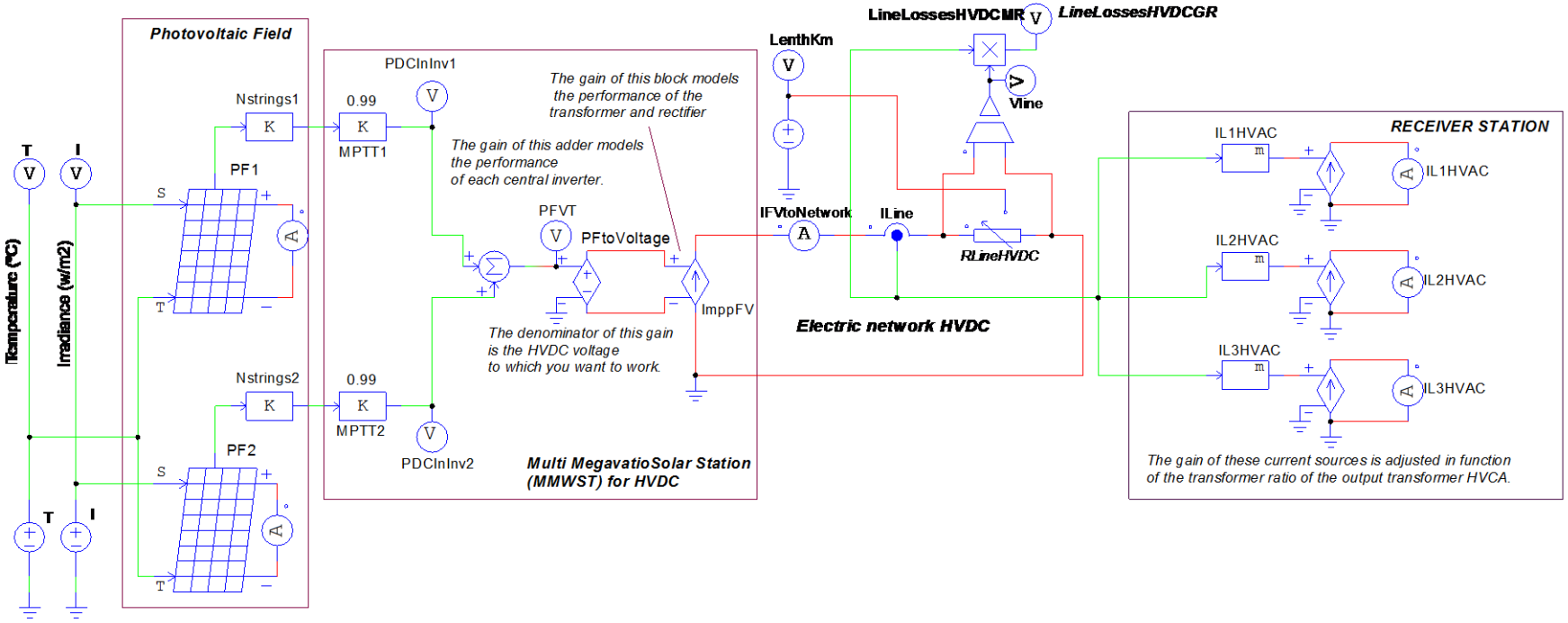

Fig. 2 Complete MMW PV plant to HVDC Model [Self-developed]

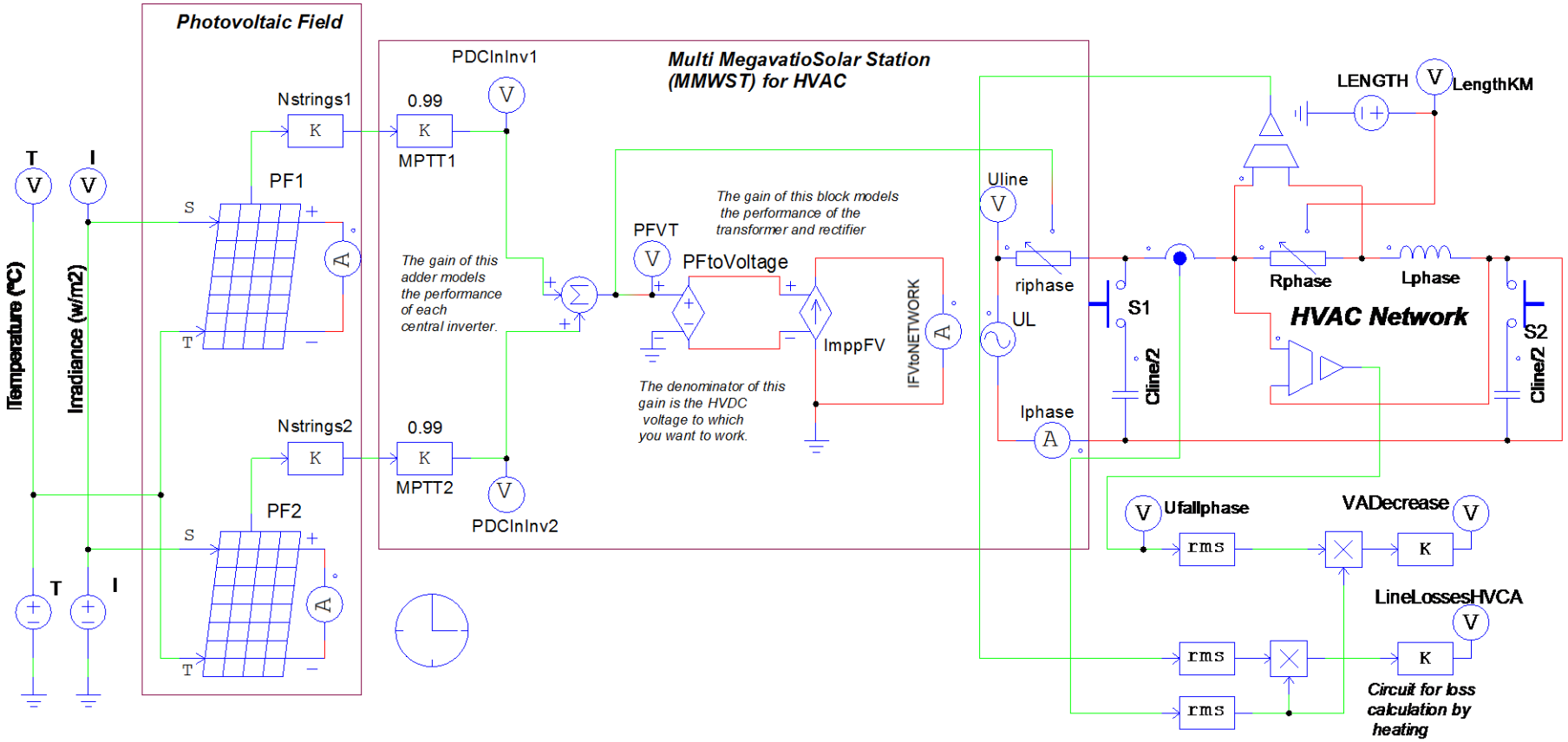

Fig. 3 Complete MMW PV plant to HVAC Model [Self-developed]

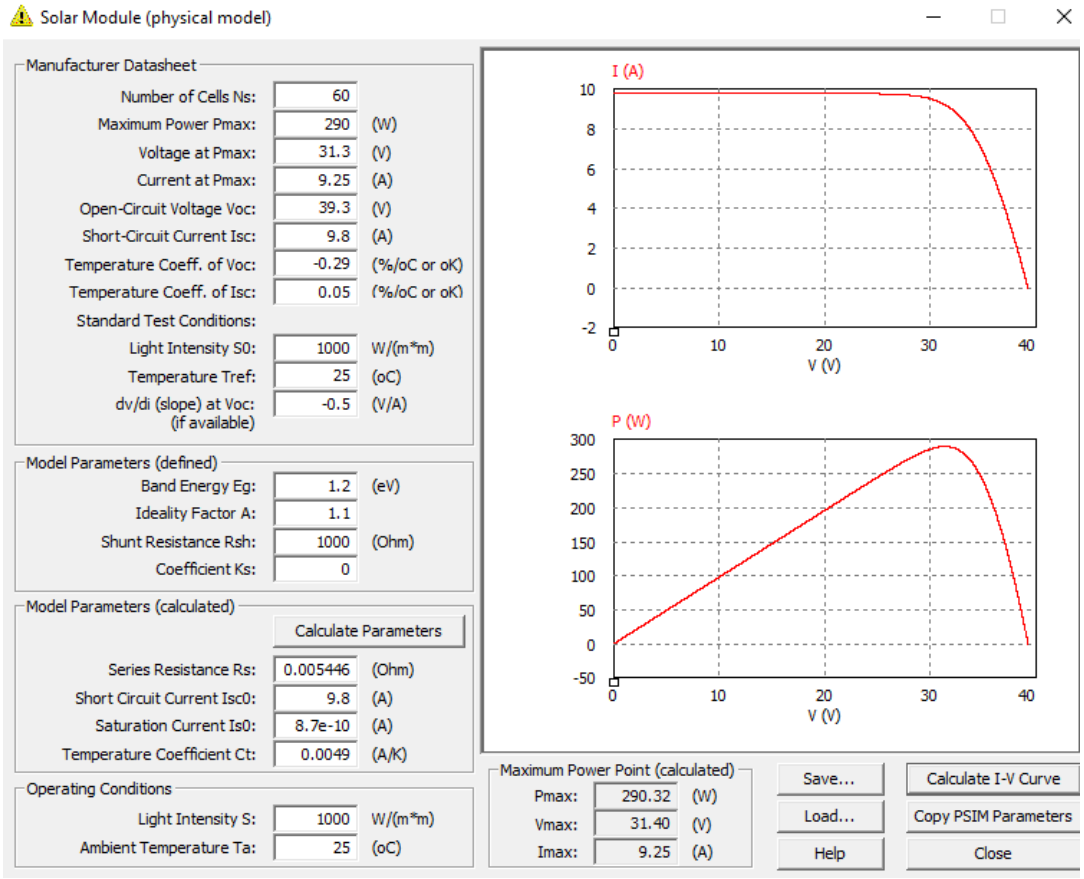

Fig. 4 Parameterization of the UN-RC290 module with the Solar Module (Physical Model) tool. [Self-developed]

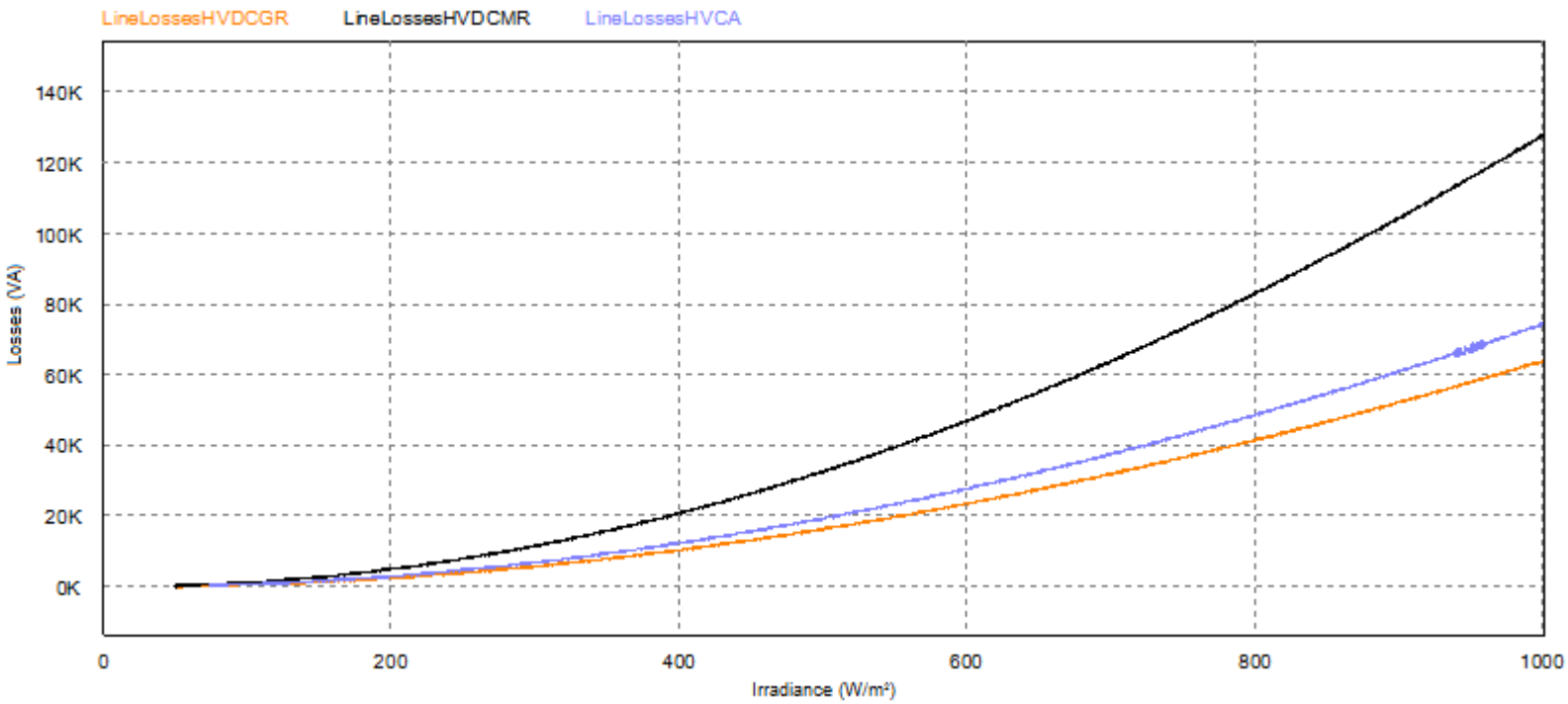

Fig. 5 Losses due to Joule effect according to Irradiance, Tº = 25ºC, l = 80km, underground [Self-developed]

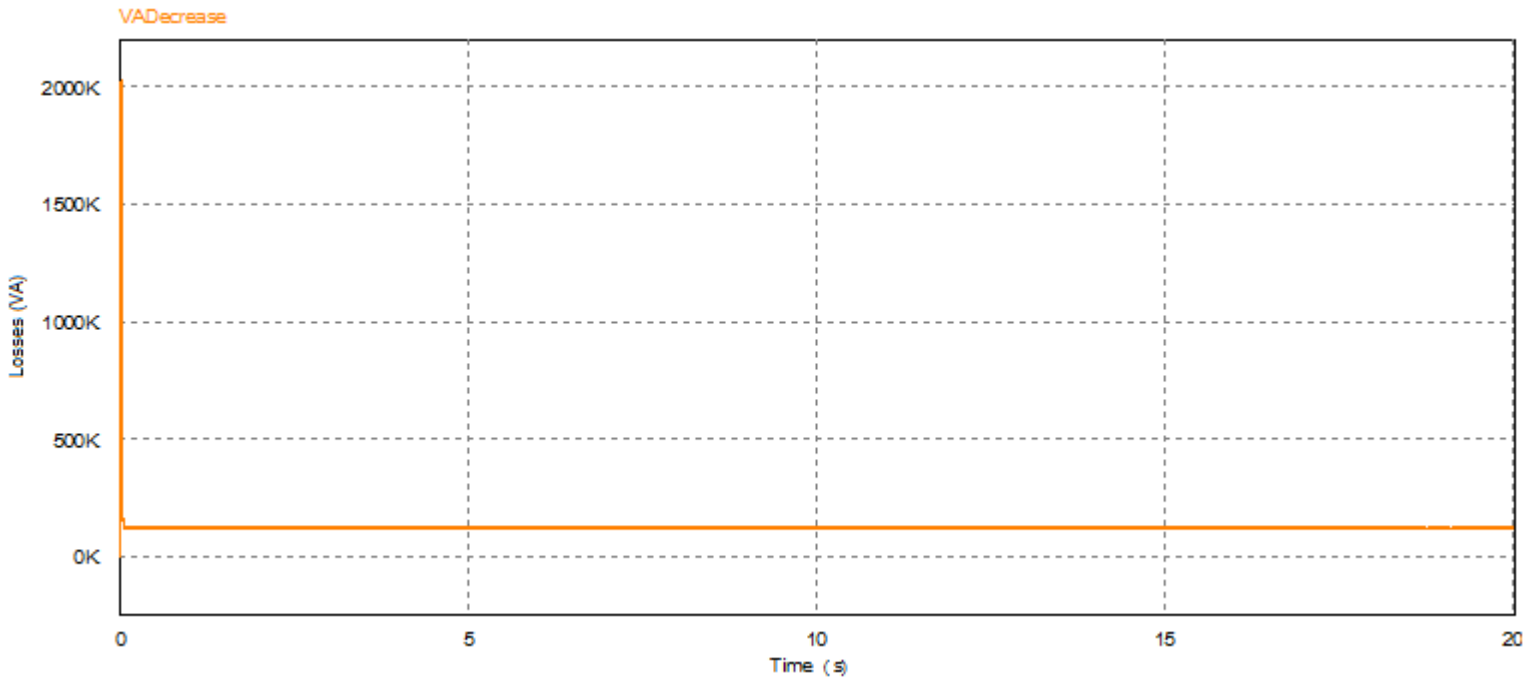

Fig. 6 Decrease in line capacity HVAC under STC, I = (1000W/m^2), T^o = 25 ºC and l = 80 km underground [Self-developed]

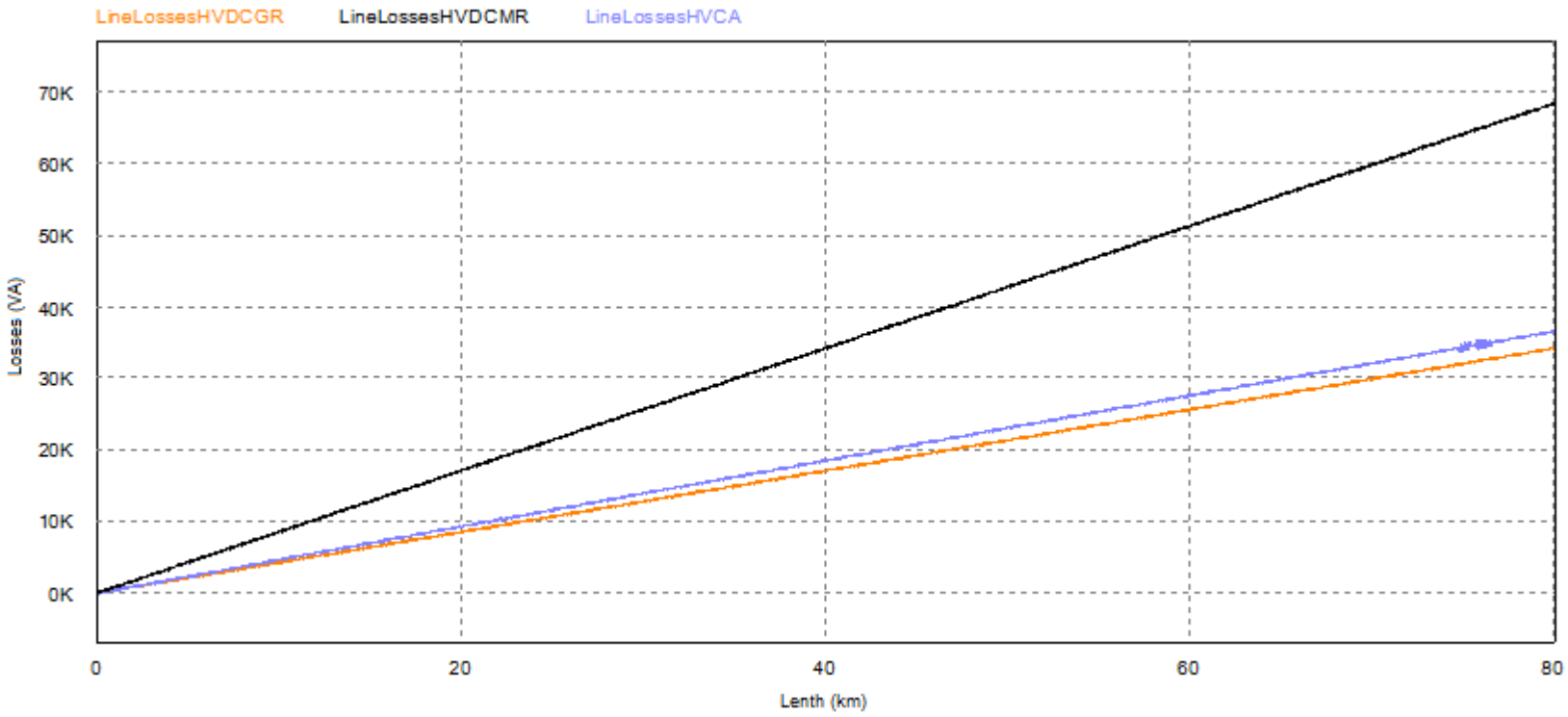

Fig. 7 Joule effect losses as a function of length, aerial network and NOCT, T^{o} = 48 ºC, I = 800 (W/m^2) [Self-developed]

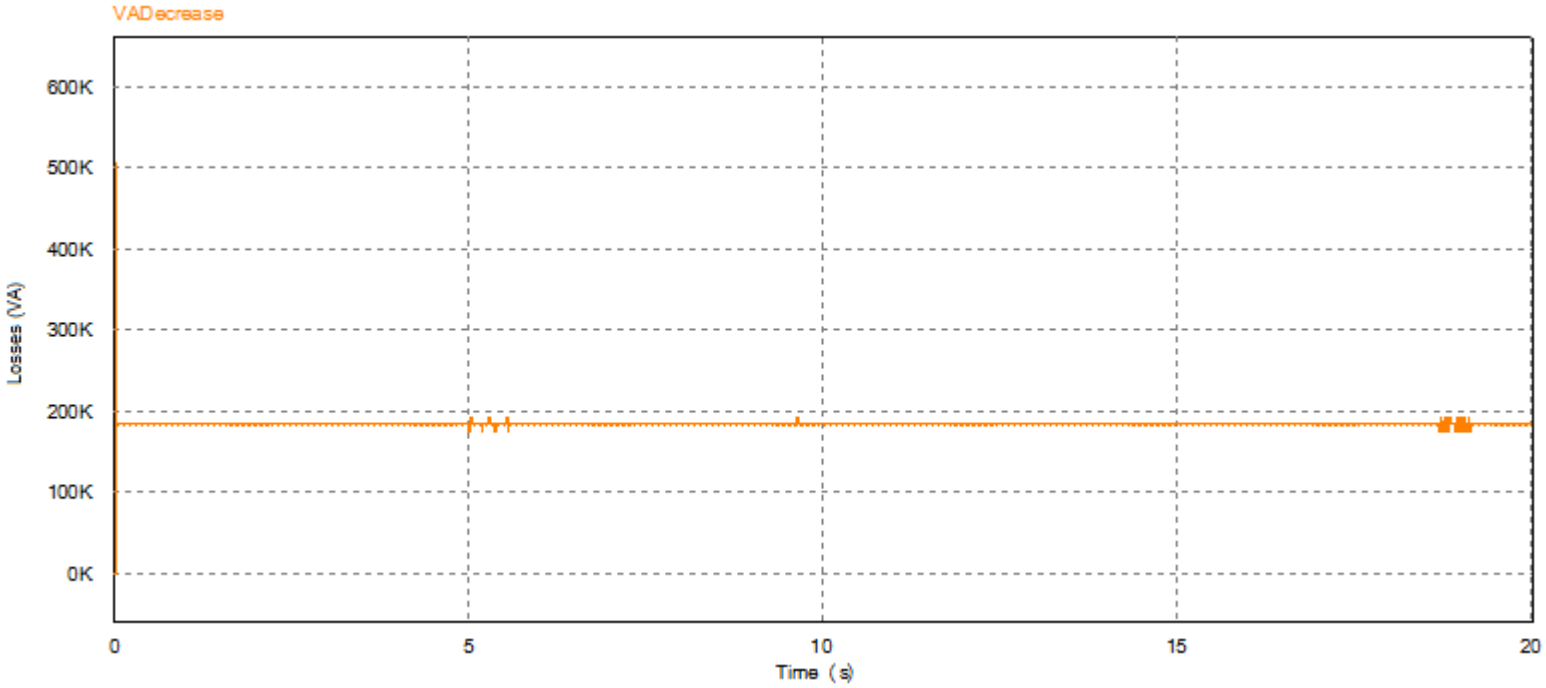

Fig. 8 Decrease in line capacity HVAC, aerial network and NOCT, T^{o} = 48 ºC, I = 800 (W/m^2) [Self-developed]

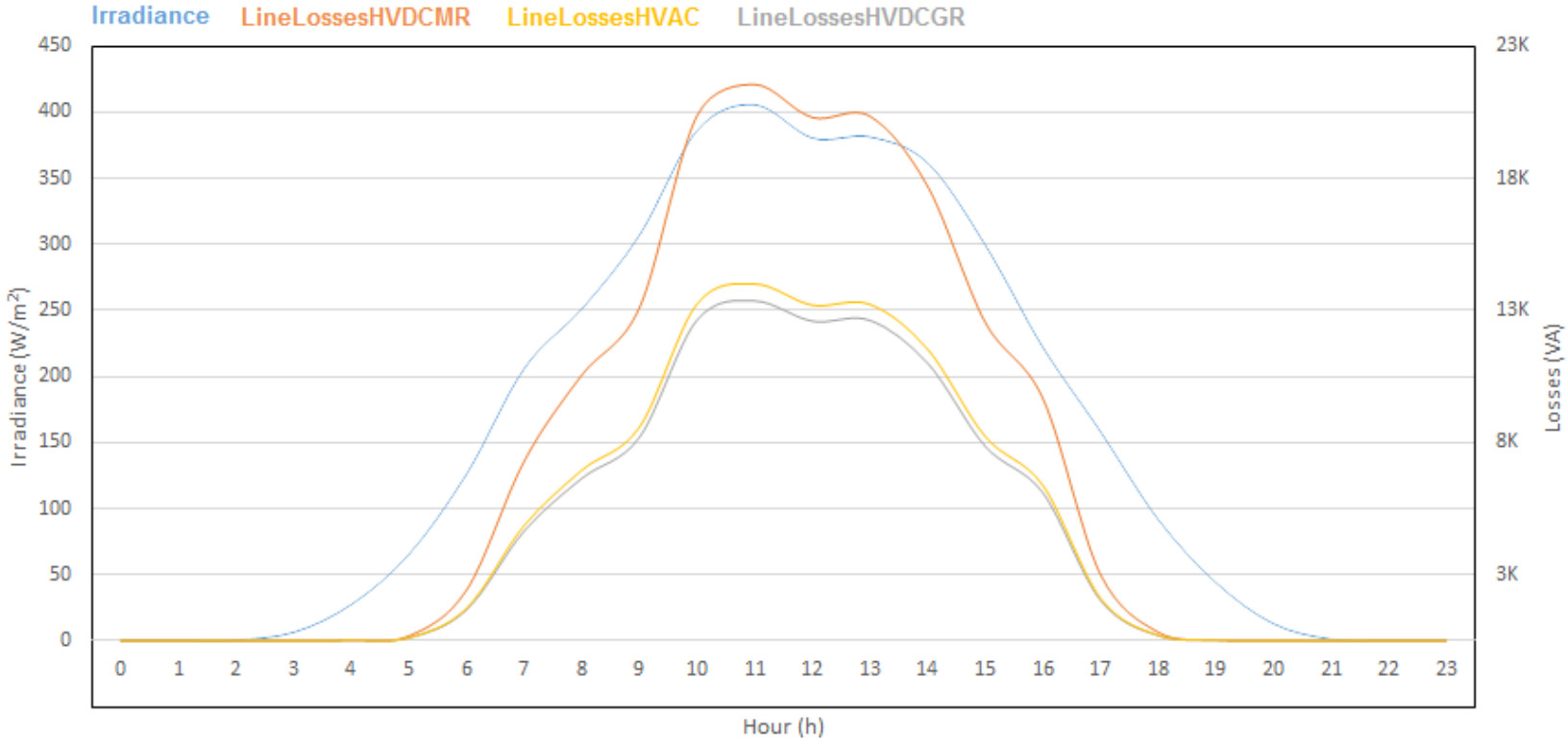

Fig. 9 Losses due to Joule effect according to hour, underground, in the month of July in the Shetland Islands [Self-developed]

Table

TABLES

TABLE I
PV MODULE REQUIRED PARAMETERS [19]

PARAMETERS TO BE DEFINED	
Band Energy Eg	eV
Coefficient Ks	No units
Ideality Factor A	No units
Shunt Resistance Rsh	Ω
PARAMETERS TO BE CALCULATED	
Series Resistance Rs	Ω
Saturation Current Is0	A
Short Circuit Current Isc0	A
Temperature Coefficient Ct	A/°C o K

TABLE II INPUT VARIABLES AND INDICATORS FOR THE HDVC MODEL [Self-developed]

NAME	FUNTION	UNIT
Irradiance (Voltage Source)	Irradiance adjustment	W/m^2
µ CC/CA (In block adder)	AC/DC Converter Performance adjustment	No unit
µ MPTT (in proportional block)	MPPT block performance adjustment	No unit
µ Transformer (Voltage-controlled current sourc	Transformer performance adjustment	No unit
IFVtoNetwork (Current Probe)	PV current to network	A
IL1HVAC (Current Probe)	AC current to HVAC network (phase 1)	A
IL2HVAC(Current Probe)	AC Current to HVAC network (phase 2)	A
IL3HVAC(Current Probe)	AC Current to HVAC network (phase 3)	A
Irradiance, I (Voltage Probe)	Irradiance indicator	W/m^2
LenthKm (Voltage Probe)	HVDC link length indicator	km
Lenthkm (Voltage Source)	HVDC length adjustment	km
LineLossesHVDCGR(Voltage Probe)	HVDC GR voltage drop	W
LineLossesHVDCMR (Voltage Probe)	HVDC MR voltage drop	W
N° Strings (in proportional block)	PV Field adjustment	No unit
PDCInInv1 (Voltage Probe)	DC power produced by converter 1	W
PDCInInv2 (Voltage Probe)	DC power produced by converter 2	W
PPVT (Voltage Probe)	Power in DC produced by all converters	W
RLineHVDC	HVDC link resistance	Ω
Temperature (Voltage Source)	PV Module operating temperature adjustment	°C
Temperature, T (Voltage Probe)	PV Module operating temperature indicator	°C
VHVDC (Voltage-controlled voltage source)	HVDC link voltage	V
Vline (Voltage Probe)	HVDC link voltage drop	V

TABLE III INPUT VARIABLES AND INDICATORS FOR THE HDAC MODEL [Self-developed]

NAME	FUNTION	UNIT
µ CC/CA (In block adder)	AC/DC Converter Performance adjustment	No unit
µ MPTT (in proportional block)	MPPT block performance adjustment	No unit
µ Transformer (Voltage-controlled current sourc	Transformer performance adjustment	No unit
Cline	HVAC capacitance	µF
IFVtoNetwork (Current Probe)	PV current to network	A
Iphase	HVAC link current (per phase)	A
Irradiance (Voltage Source)	Adjust irradiance level	W/m^2
Irradiance, I (Voltage Probe)	Irradiance indicator	W/m^2
LenthKm (Voltage Probe)	HVAC link length indicator	km
Lenthkm (Voltage Source)	HVAC link length adjustment	km
LineLossesHVAC (Voltage Probe)	Loss of power in the HVAC link	W
Lphase	HVAC link inductance (per phase)	mH
N° Strings (in proportional block)	PV Field adjustment	No unit
PDCInInv1 (Voltage Probe)	DC power produced by converter 1	W
PDCInInv2 (Voltage Probe)	DC power produced by converter 2	W
PFVT (Voltage Probe)	Power in DC produced by all converters	W
riphase	HVAC internal resistance (per phase)	Ω
Rphase	HVAC resistance (per phase)	Ω
S1, S2	Allows to take into account or not the capacitive	No unit
Temperature (Voltage Source)	PV Module operating temperature adjustment	°C
Temperature, T (Voltage Probe)	PV Module operating temperature indicator	°C
VADecrease	HVAC link dimished capacity	VA
VFallPhase (Voltage Probe)	Voltage drop per phase on the HVAC link	V
Vline	RMS line voltage on the HVAC link	V

TABLE IV

TRANSMIT LOSSES FOR EACH TYPE OF LINK [Self-developed]

CASE	HVDC GROUND RETURN		HVDC METALLIC RETURN		HVAC 3-PHASE			
U:UND; A:AIR	JOULE LOSSES		JOULE LOSSES		JOULE LOSSES		DECREASE CAPABILITY	
T° (°C)/I (Wm2)	J L (W)	J L (%)	J L (W)	J L (%)	J L (W)	J L (%)	DC (VA)	DC (%)
UNDERGROUND NETWORK: Insulated cables (Aluminum, S=500mm2, XL=0,095(Ω/Km), C=484(μF/Km))								
U -10/1000	83.304,03	4,17%	166.608,06	8,33%	96.541,92	4,83%	161.498,98	8,07%
*U25/1000	64.001,00	3,20%	128.002,39	6,40%	74.599,95	3,73%	124.788,99	6,24%
**U 48/800	34.240,00	1,71%	68.480,00	3,42%	40.350,05	2,02%	67.496,58	3,37%
U 70/1000	42.409,77	2,12%	84.819,54	4,24%	48.809,60	2,44%	83.320,29	4,17%
AERIAL NETWORK: Cables without isolation (Aluminum, S=500mm2, XL=0,35(Ω/Km), C≈0)								
A -10/1000	83.304,03	4,17%	166.608,06	8,33%	87.328,48	4,37%	440.180,00	22,01%
*A 25/1000	64.001,00	3,20%	128.002,39	6,40%	67.592,28	3,38%	340.700,00	17,04%
**A 48/800	34.240,00	1,71%	68.480,00	3,42%	36.647,89	1,83%	184.724,40	9,24%
A 70/1000	42.409,77	2,12%	84.819,54	4,24%	45.210,80	2,26%	227.885,92	11,39%
*Figures 5 to 8 belong to the shaded cases .*STC Standard test conditions, **NOCT Normal Operating Cell Temperature*								